CALCULATED LITHOSPHERIC STRENGTH ENVELOPES: IMPLICATIONS FOR UNDERSTANDING ELASTIC AND SEISMOGENIC LAYER THICKNESSES ON MARS

Paul Morgan[1,*], Alex. Batov[2,3], Adrien. Broquet[4], Tamara Gudkova[2], Scott King[5], Francis Nimmo[6], R.T. Ratheesh Kumar[7,8], Dhananjay Ravat[8], Suzanne S. Smrekar[9] and Martin van Driel[10]

[1]Colorado Geological Survey, Colorado School of Mines, 1801 Moly Rd. Golden, CO 80401, USA. [2]Schmidt Joint Institute of Physics of the Earth, Russian Academy of Sciences, B Gruzinskaya 10, Moscow 123242, Russia. [3]also at Trapeznikov Institute of Control Sciences, Russian Academy of Sciences, Ulitsa Profsoyuznaya, 65, Moscow, 117997 Russia. [4]Université Côte d'Azur, Laboratoire Lagrange, Observatoire de la Côte d'Azur, CNRS, Nice, France. [4]Department of Geosciences, Virginia Tech, Blacksburg, VA, USA. [5]Department of Earth and Planetary Sciences, University of California, Santa Cruz, Santa Cruz, USA. [6]Department of Earth and Environmental Sciences, University of Kentucky, Lexington, KY 40506, USA, [7]on leave from Department of Marine Geology and Geophysics, School of Marine Sciences, Cochin University of Science and Technology, Kochi- 682016, India. [8]Jet Propulsion Labotatory, California Institute of Technology, Pasadena, CA, USA. [9]Institute of Geophysics, ETH Zurich, Zurich, Switzerland.

Corresponding author: Paul Morgan (morgan@mines.edu)

*Authors listed in alphabetical order after Morgan

Key Points:

- Published elastic and seismogenic thicknesses for Mars determined by different methods do not all represent the physical parameter;
- They can be related through calculated lithospheric strength envelopes;
- InSight marsquake results combined with these parameters yields a cleared physical understanding of the Mars lithosphere.

Complete author addresses and Orcid numbers are being collected – I apologize that they were not available at time of submission.

Suggested reviwers:

Walter S. Kiefer, LPI, Houston, TX
Roger Phillips, retired, Boulder, CO
Mark Wieczorek, Nice, France

Abstract

Calculated lithospheric strength envelopes (*LSE*s) are rheological models of the lithosphere that are useful in understanding the elastic (T_e) and seismogenic (T_s) thicknesses of the lithosphere. Determinations of Te for Mars using different techniques use different models of Te as indicated by rheology in LSEs, and LSEs indicate that the differential stress fields that cause deformation must be considered in the determination of both Te and Ts. We do not attempt to review the literature here or to rank different methods. Our goal is to provide a better understanding of the different values of Te and Ts published in the literature and to encourage integration of these data with a physical understanding of the lithosphere in time and space.

Plain Language Summary

Different techniques used to measure the strength of the outer shell of Mars as it has deformed under loads, primarily large volcanoes, have measure different aspects of this strength. Different methods of predicting the maximum depths that earthquakes should occur have also measured different quantities. Using a theoretical model supported by laboratory experiments of how ths shell should deform and allow earthquakes at different depths, we can compare the different techniques that predict these quantities. Our goal is to provide a better understanding of the different quantities that are measured so that they may be used to understand the physical properties of the shell. This understanding is combined with new marsquake results from the InSight Mars lander mission to study the shell in the region around the landing site.

1 Introduction

InSight is a Mars lander representing the first planetary robotic exploratory mission to study the interior of Mars in detail. Important to this study are not only interpretations of data collected by the lander but also integration of the new data and interpretations with results and information derived from previous missions and studies, including studies of Mars evolution and structure made in association with the InSight mission before landing. Some of these studies have included derivation of the mechanical properties of the Mars' lithosphere, including its elastic strength associated with the support of long-term stresses and its seismogenic layer depththat is generally taken to be depth limit for the generation of earthquakes. These parameters are interrelated by theoretical models of the lithosphere generally known as Lithospheric Strength Envelopes (*LSEs*). *LSEs* allows estimation of the effective elastic thickness of the lithosphere, T_e, and the thickness of the seismogenic layer, T_s, if a simplified layered composition of the lithosphere, strain rate, and geotherm (heat flow) are known, or may be assumed, together with laboratory measured rock properties (*e.g.*, Burov and Diament, 1995). One of the science goals of the InSight mission is to understand the formation and evolution of Mars with the ultimate ambition of uncovering how a rocky body forms and evolves to become a planet. As part of that goal, this contribution seeks to provide a common framework for published and new studies of T_e and T_s to assist in understanding the tectonic evolution of the Mars lithosphere.

*LSE*s are calculated curves that model the yield strength of the lithosphere as a function of depth. They have been used studies of the rheology of the Mars lithosphere since at least the 1990s (*e.g.*, Solomon and Head, 1990). However, as they are the main focus of this discussion,

their calculation as used in the present study is given in the Appendix. A good, brief introduction to T_e and T_s on Mars was given by Grott et al. (2013). The main focus of the body of the text here will be the parameters that control *LSE*s, and an examination of T_es and T_ss derived from different methods. This is NOT a review article and we have made no attempt to rank different methods or results. Our goal is to provide a basis and an understanding that published values of T_e and T_s may not describe the same lithospheric properties but they are all valuable if the constraints of the methods are understood.

2. Principal controls on Mars' *LSE*s

Specific parameters used in the calculation of *LSE*s are discussed in the Appendix but they may be summarized into three controlling factors for *LSE*s on Mars: 1) crustal thickness; 2) heat flow/geotherm; and 3) strain. The martian crust is interpreted to be a primarily basaltic crust with little, if any, significant volume of tertiary crust (Taylor and McLennan 2009). The main crustal variable then is thickness. There are two ways that crustal thickness changes lithospheric rheology. Firstly, crustal compositions are much weaker than mantle compositions for ductile deformation. Therefore, thicker crust generally has a weaker *LSE*. Secondly, crustal compositions have a lower thermal conductivity and higher radiogenic heat production than mantle compositions which tend to lower the geotherm for the same surface heat flow, somewhat counteracting the first effect on the *LSE* of the mechanically weaker crustal material. The integrated strengths to a depth of 250 km of *LSE*s with crust of 30 and 60 km are shown in Figure 1 as a function of surface heat flow. The integrated strengths of *LSE*s for both crustal thicknesses are equal up to a heat flow of about 10 mW/m^2 because there is no ductile deformation in the rheology and the integrated strength is arbitrarily limited by the depth limit of 250 km. This equality is artificial because they would both rise to higher values if the integrations were to continue to greater depths, but the maximum thickness of the Mars lithosphere is not known. As surface heat flow increases, the integrated strength of the 30 km crust lithosphere starts to decrease first because its geotherm is slightly lower than the thicker crust geotherm and strength starts to be lost first in the lowermost layers of the 250 km lithosphere (Appendix). This continues until the surface heat flow is about 60 mW/m^2 when the mantle strength is depleted, main strength loss is in the crust and the rate of strength loss decreases. The integrated strength of the 60 km crust *LSE* decreases more rapidly than the 30 km crust *LSE* from about 15 to 30 mW/m^2 because the increasing geotherm results in ductile deformation in both the lower layers of both the mantle lithosphere and the crust (Appendix). Between about 30 and 40 mW/m^2 almost all of the strength remaining is ductile strength in the crust and at about 60 mW/m^2 the 30 and 60 km thick crust models predict equal integrated strengths because all remaining strength is in the crust above 30 km.

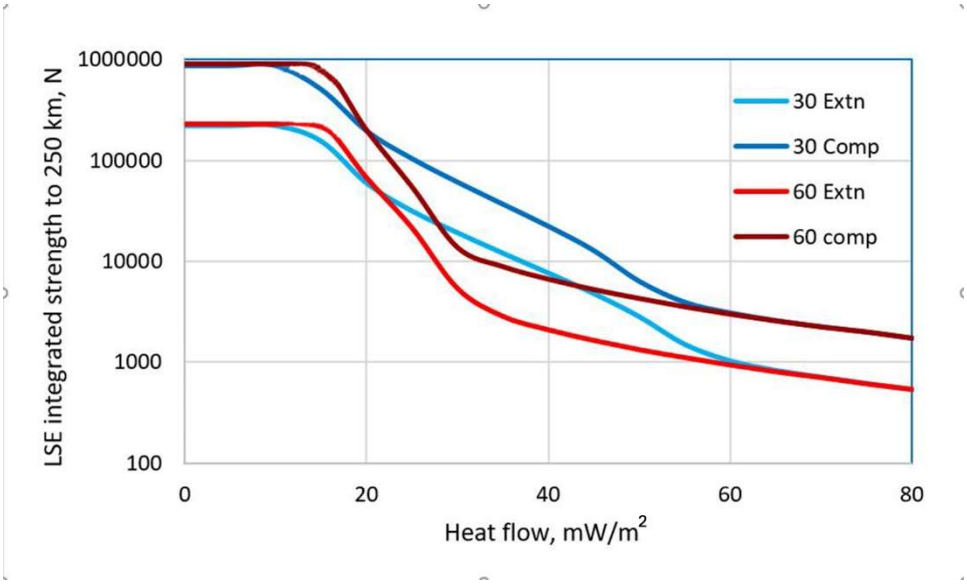

Figure 1. Integrated lithospheric strength envelopes calculated to a depth of 250 km for lithospheres with a 30 and 60 km-thick crusts. Flattening of curves on left is artificial and is a result of the integration stopping at a depth of 250 km. B. Same as A, but integrations from curves shown in Figure A4. Curves for 30 km crust are shown in blue and for 60 km crust are shown in red. extn indicated lithosphere under extension, comp indicates lithosphere under compression.

Figure 1 also demonstrates the significance of heat flow, or more specifically the geotherm on *LSE*s (Appendix). Many papers have studied the thermal and crustal evolution of Mars (*e.g.*, Hauck & Phillips, 2002; Guest & Smrekar, 2007; Grott & Breuer, 2008; Morschhauser et al., 2011; Grott et al; 2013; Plesa et al, 2015). These studies have different purposes, ranging from constraining the bulk crustal and volatile evolution of Mars to determining the global average geotherm for Mars as a function of time to studying the volcanic history of Mars. They clearly illustrate that heat flow in Mars has changed in time and space during the evolution of Mars. Kiefer and Li (2009), among others, have shown that even simple models of a mantle plume of the type that is commonly thought to be associated with the major volcanic centers on Mars, such as Tharsis, controls lateral variations in lithospheric thickness and T_e. Plesa et al. (2016) have addressed the question, "How large are present-day heat flux variations across the surface of Mars?" Their answer is that the largest peak to peak variations lie between 17 and 50 mW/m^2, with an average between 23.2 and 27.3 mW/m^2. As the planet is cooling, the high end of the peak to peak variations and the average are probably higher. However, here may be a limit to the upper end of the range after initial crust formation.

The highest published terrestrial continental heat flow is 15,600 mW/m^2, measured in lake sediments near a geothermal vent in Yellowstone Lake in the Yellowstone Caldera, Wyoming, USA (Morgan et al, 1977). Temperatures in these sediments were buffered by the water boiling-point curve. Morgan et al. suggest a silicic magma chamber underlies this caldera and temperatures in the crust at this and similar locations are buffered by the crustal solidus. Thus, although average heat flow, and probably average upper mantle temperatures were higher in the

ancient earth, it is unlikely that local continental heat flow and geotherm conditions were higher in the past than in the geologically recent evolution of the Yellowstone caldera. Terrestrial large igneous provinces (LIPs, *e.g*., Bryan and Ernst, 2008) may be somewhat analogous to the basaltic magmatism on Mars. These magmas originate in the upper mantle, are low viscosity and do not form large shallow magma chambers. Areas of voluminous young basaltic volcanism of earth without a more silicic component are not characterized by significantly high surface heat flow but elevated mantle heat flow (*e.g*. Columbia River Basalts, Columbia Plateau, USA; Blackwell et al., 1978). Their surface heat flow is not significantly elevated relative to other continental areas because the high volume of basalt in the crust is low in radiogenic heat production relative to less mafic terrestrial crust. On Mars they would be expected to have relatively high surface heat flow while active because heterogeneity in crustal heat production is probably minor compared with lateral variations in mantle heat flow. A very rough estimate of Mars peak heat flow may be made by assuming that basaltic magma ponds at the base of the crust-mantle boundary for a sufficiently long time for temperatures in the overlying crust to equilibrate. Assuming a magma temperature of 1475 K, a surface temperature of 220, crustal thickness of 30 km and a crustal thermal conductivity of 2 W/(m K) (Beardsmore and Cull, 2001), the peak thermal gradient would be ~42 K/km and heat flow ~84 mW/m^2. If the crustal thickness is increased to 60 km, the gradient is reduced to ~21 K/km and heat flow to 42 mW/m^2. These values bracket the peak current heat flow of 50 mW/m2 predicted by the models of Plesa et al. (2016), and provide a buffering mechanism why heat flow significantly higher than about 80 mW/m^2 is unlikely after the primary crust of Mars was formed.

Strain is the third principal controlling factor of *LSE*s. Firstly, strain rate is an important parameter in calculating ductile strength. On earth, where plate tectonics allows relatively rapid movements among plates and between plates and the underlying asthenosphere, a strain rate of the order of 10^{-15} s^{-1} is commonly assumed. Mars is generally assumed, and its thermal evolution and crust generation are best explained as a one-plate planet (e.g., Breuer and Spohn, 2003) with movements restricted to deformation within the plate. Strain rates ranging from of 10^{-14} to 10^{-19} s^{-1} has been assumed when calculating ductile strength (McGovern et al., 2002, 2004; Plesa et al., 2016; see Appendix). Secondly, when considering T_e or T_s, these parameters are not predicted directly from the *LSE*. The type of strain at any depth, brittle, elastic, ductile, or some combination of the three, is predicted by the interaction of the external differential stress with the *LSE*, a changing stress with depth caused by flexure of the lithosphere or a uniform stress with depth caused by a remote extensional or compressional stress As shown in the Appendix, how the external differential stress interacts with the *LSE* is used to define T_e and T_s and results in significantly different portions of the area of the *LSE* being used to calculated elastic strength and sections of the brittle curves at different depths being considered a potential depths for seismicity.

In addition, although calculation and use of *LSE*s usually assumes that stresses are applied instantaneously to the lithosphere and that the shape of the resulting *LSE* does not change with time, the shape of the *LSE* does change with time and the speed at which stresses are applied to the lithosphere (*e.g*., Bott and Kusnir, 1984; Kusnir and Park, 1984; Albert et al., 2000). Brittle strength does not change with time but ductile sections of the lithosphere relax differential stresses under which they are subjected and these stresses are concentrated in the brittle

lithosphere. This transient behavior is rarely considered in the published literature and its application is limited by other uncertainties in parameters used in calculating *LSE*s. No further consideration of transient creep modifying *LSE*s will be made here.

3. Different methods for determination of T_e for Mars

In this section we discuss some of the different methods used to calculate T_e for Mars, their relations, if any, with *LSE*s and the relative magnitudes of the T_es determined by the different methods. These methods fall into three basic categories: 1) admittance in which gravity and topography are used to model bending of an elastic plate; 2) use of *LSE*s in which the a low-viscosity limit in the ductile portion of the mantle portion of the *LSE* is used to define T_e (also called the thickness of the mechanical lithosphere, T_m; *e.g.*, Grott et al., 2013); and 3) use of *LSE*s in conjunction with fault spacing and depth penetration and either flexure induced by a load or deformation from an external in-plane stress (see Appendix).

McGovern et al. (2002, 2004) used gravity/topography admittances to estimate the thickness of the martian elastic lithosphere (T_e) required to support the observed topographic load since the time of loading (Albert and Phillips, 2000). They made calculations with different assumptions of crustal density, subsurface loading and crustal ductile composition which had significant consequences to their calculated T_e values. Their results are summarized in Table 1. The most general conclusion that may be taken from these results is that T_e is smaller for Noachian loads than for younger loads. Changes in assumptions with the method, such as the addition of bottom loading in the solution for Hellas south rim, as could occur from ponding of basaltic magma at the crust-mantle interface, result in major changes in the estimate of T_e.

Plesa et al. (2016) calculated present-day heat-flow variations across the surface of Mars and used these data to calculate a global map of T_e. They approximated T_e by the mechanical thickness of the lithosphere, the depth corresponding to the temperature at which the *LSE* indicates a loss of mechanical strength due to ductile flow (Appendix). Following Burov and Diament (1995) and Grott and Breuer (2010), they take this bounding strength at 10 MPa (in contrast McNutt, 1984, defined the base of the plate in terms of *LSE*s as the depth at which the stress difference is less than 50 MPa). Thus, they used the *LSE* formalism, but took T_e as the greatest thickness of the *LSE* at which the maximum yield strength dropped below 10 MPa. Another difference to the calculations to the calculations presented in the Appendix is that they used a strain rate for ductile strength calculations of 10^{-14} s^{-1}, which is at the high end of strain rates commonly used for Mars ductile strain calculations (see Appendix). 10^{-14} s^{-1} may be an appropriate strain rate for glacial loading at the martian North Pole, and perhaps even in the convecting mantle, but is probably high for most deformation in the Mars' lithosphere. Even with terrestrial plate tectonics a strain rate an order of magnitude lower (10^{-15} s^{-1}, *e.g.*, Burov, 2011) is generally used for *LSE* calculations and without plate tectonics on Mars the global strain rate is probably much less. However, a uniform lower strain rate in the calculations would lower all lithospheric thickness estimations but would not significantly change relative thickness estimations.

An additional feature of using a temperature-defined rheology to determine the thickness of the elastic lithosphere so derived is tied to the age of the geotherm use to calculate the rheology. For example, Azuma and Katayuma (2017) calculated global average geotherms at intervals of 1 Ga

since 4 Ga before present and used these geotherms to calculate *LSE*s for the Mars North Pole and Solis Planum (see also Appendix). As noted by Albert and Phillips (2000) values of T_e that are calculated from deformation of the lithosphere by loading are primarily relevant to the geotherm at the time of loading unless a subsequent larger thermal event and/or loading results in later deformation. Thus, if the global average geotherms calculated by Azuma and Katayuma (2017) were representative of Olympus Mons at the time of its eruption and loading of the lithosphere (unlikely), the *LSE* from this geotherm would yield an appropriate T_e. The T_e variations from the global map of Plesa et al (2016) were derived from geotherms that may not have been the highest geotherms in the lithosphere for most regions on Mars. If the convection system in the Mars interior has remained stable since crust formation so that mantle plumes have remained stationary relative to the crust, there has probably been some secular cooling in the planet so that all geotherms have decreased. Under these circumstances T_e would be overestimated at all locations by the Plesa at al. map. A more probable model is that the Mars convection system slowly changed through time so that surface heat flow variations for the present-day modeled by Plesa et al. (2016) is a snapshot in time. The distribution of variations in surface heat flow would slowly change with the thermal evolution of the Mars lithosphere. If the present-day variation in surface heat flow do not represent the distribution of heat-flow variations on time scales of hundreds of millions of years, the T_e map generated from the present-day heat flow variations may differ from T_e values calculated from deformation by loading of the lithosphere earlier than Late Amazonian.

Deformation of the lithosphere either by flexure or plane strain can link T_e and *LSE*s. A lithospheric strength envelope is a diagram that indicates in a simplified form the type of yield strain that may be expected at different depths if the differential yield strength is exceeded at a specified depth. Up to the yield strength, strain is assumed to be primarily elastic. The area encapsulated by the *LSE* is therefore an indication of the potential elastic strength, but this elastic strain can only be activated by deformation within the elastic field of yield strength. As discussed in the Appendix, convex up flexure causes extension in the upper part of the lithosphere and compression in the lower part of the lithosphere; extension and compression are reversed in the lithosphere for concave up flexure. These flexure stresses were discussed with respect to an *LSE* by McNutt (1984) and she gave a formal relationship between T_e as defined by flexure of an elastic plate and the approximate base of the plate, where z = T_m, where stress differences are less than 50 MPa. This relationship is shown in Figure 2. Although the *LSE* is probably a more realistic model of the rheology of the lithosphere, T_e was defined from the elastic plate model. There is not a simple analytical relationship between the areas defined by the stress difference in the elastic plate mode and the *LSE*: Burov and Diament (1995) discuss the elastic strength for the *LSE*, but end with a numerical solution. Watts and Burov (2003) and related references have given the general relationship between these two T_es as:

$$T_e(LSE) \approx T_e(\text{elastic}) C(K,t,h_1,h_2,\ldots) \quad (1)$$

where C is a function of the curvature of the lithosphere, K, the thermal age, t (the age of loading), and the thicknesses of layers of different compositions in the lithosphere, h_1, h_2, etc. (see Appendix). Thus, the ratio of $T_e(LSE)$ to T_e(elastic) varies according to the load, the age of the load, the geotherm at the time of the load, and the lithospheric structure at the location of the load, and this ratio is variable. An important result of dependence on the load with that $Te(LSE)$ varies with curvature of the flexure (*e.g.*, Burov and Diament, 1995).

a) b)

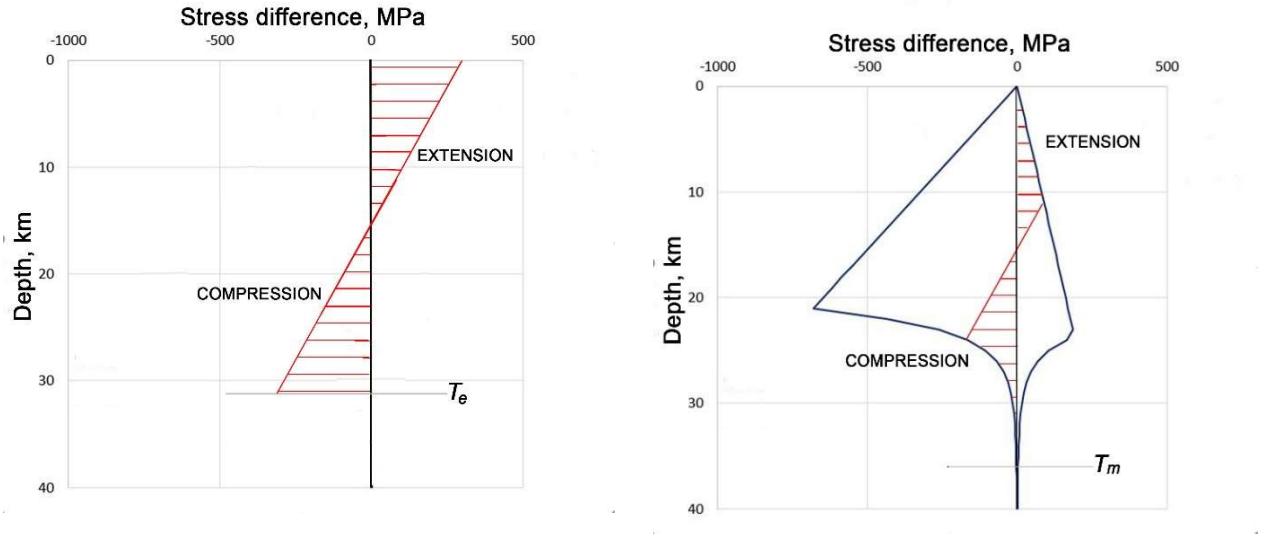

Figure 2. Differential stresses exerted on lithosphere by flexure: A. assuming thin elastic plate model; assuming LSE model. Horizontal lined areas indicate stresses. Modified from McNutt (1984).

Fault spacing and penetration have been used in a number of studies to evaluate the rheology of the martian lithosphere (*e.g.*, Comer et al., 1985; Kronberg et al, 2007). These studies relate flexure of the lithosphere with the faulting. They cover tectonic features ranging from extensional faults and graben circumferential to volcanic loads and rifting associated with regional uplift and volcanism. Comer et al. (1985) used radii of circumferential graben to large volcanic loads to calculate the thickness of the elastic lithosphere: their results are summarized in Table 2. There is some overlap in the features to which these results apply and the features studied by McGovern et al. (2002, 2004) summarized in Table 1. There are large error limits in both sets of results, but the T_es from all features fall within the overlapping uncertainties of the two sets of results. These two data sets are direct measures of T_e.

Kronberg et al. (2007) modeled tectonic rifting and volcanism and the Noachian Acheron Fossae using finite elements to determine the elastic properties of the lithosphere from flexure, and used *LSE*s to determine the geotherm from these results. A number of other studies have used *LSE*s to relate heat flow and or the geotherm to elastic properties of the lithosphere, but, as discussed above, the relations are not exact if the elastic property, Te, is the elastic lithosphere determined from plate flexure models. Kronberg et al. (2007) used the equation:

$$T_e = \left(\frac{12(1-\nu^2)M_{LSE}}{KE}\right)^{1/3} \quad (2)$$

Where E and ν are Young's modulus and Poisson's ratio, respectively, K is curvature, and M_{LSE} is the sum of all moments associated with the brittle, elastic, and ductile parts of the *LSE*. As indicated elsewhere (e.g., Watts and Burov, 2003, equation 12), however, this formula is equal to

306 T_e(*LSE*), not T_e, and applies to oceanic lithosphere which only has one layer in its *LSE*.
307 In summary, published values of T_e for Mars come from a variety of different techniques.
308 The different techniques do not yield the same parameter. Studies of loading and lithospheric
309 flexure yield values of T_e that are closest to its original definition associated with flexure of an
310 elastic plate (*e.g.*, McNutt, 1984). However, by this method T_e may vary with the magnitude of
311 plate curvature. Other techniques that define elastic thickness through reference to rheology of
312 the lithosphere as in *LSE*s, while perhaps more physically realistic, yield values of T_e(*LSE*) that
313 are different from T_e(*elastic*). Application of *LSE*s to determine T_e is not standardized in Mars
314 publications.
315
316 **4. Relations among T_s for Mars and *LSE*s**
317 Although seismometers were included on the Viking landers in the mid-1970s, only the
318 instrument on Viking 2 operated. It was placed on the deck of the lander and was very
319 insensitive to earthquakes due to wind noise. No unambiguous earthquakes were recorded
320 (Anderson et al, 1976). However, repeated subsequent studies indicated that Mars should have
321 active seismicity (*e.g.*, Golombek et al., 1992; Phillips, 1991; Knapmeyer et al., 2006), including
322 very recent seismicity in the vicinity of the InSight landing site (Taylor et al., 2013). These
323 predictions proved correct with the detection of 174 earthquakes in 114 sols of operation of the
324 InSight seismometer. Unlike T_e, which is a derived elastic parameter, T_s, the thickness of the
325 seismogenic layer is a real thickness which, if sufficient recording instruments, favorable
326 recording conditions, and time were available, could be measured by the hypocentral depths of
327 earthquakes recorded. Theoretically, Ts may be predicted from *LSE*s as earthquakes should only
328 occur in depth segments of the *LSE* where brittle failure is indicated. Plesa et al. (2018)
329 predicted both the present-day level of Mars seismicity as a function of location on Mars and T_s
330 on a 3° by 3° grid. Although they did not formally use *LSE*s in calculating T_s values, they used
331 temperatures for the brittle-ductile transition from *LSE*s of 573, 873, and 1073 K from Phillips
332 (1991) and Knapmeyer et al. (2006). As in calculating T_e values, Plesa et al. (2018) used heat
333 flow and geotherm variations, and the same strain rate for ductile strength calculations as Plesa et
334 al. (2016). As discussed above, this strain rate of 10^{-14} s^{-1} may be too fast for the Mars
335 lithosphere resulting in high estimates for T_s. However, relative values of T_s should be useful.
336 T_s as predicted for a general Mars *LSE* is shown in Figure 3. Seismicity cannot occur unless
337 there is a differential stress that exceeds the brittle yield strength in part of the *LSE*. Figure 3
338 shows a stress difference cause by convex upward lithospheric flexure that intersect the brittle
339 yield strength in both the crust and the mantle. Earthquakes with extensional fault mechanism
340 would be expected in the upper crust and the uppermost mantle. If the flexure had the same
341 magnitude convex downward, earthquakes would occur in the upper crust, but at a shallower
342 depth, but not in the mantle because the brittle yield strength would not be exceeded below the
343 crust-mantle boundary. T_s is predicted at the maximum depth(s) where the differential stress
344 driving deformation exceeds the brittle yield strength, not at the brittle-ductile transition.
345 Hypocentral depth information are awaited from the InSight mission to determine whether the
346 brittle-ductile transitions or the differential stress-LSE intersections are the better predictors of
347 the T_s.

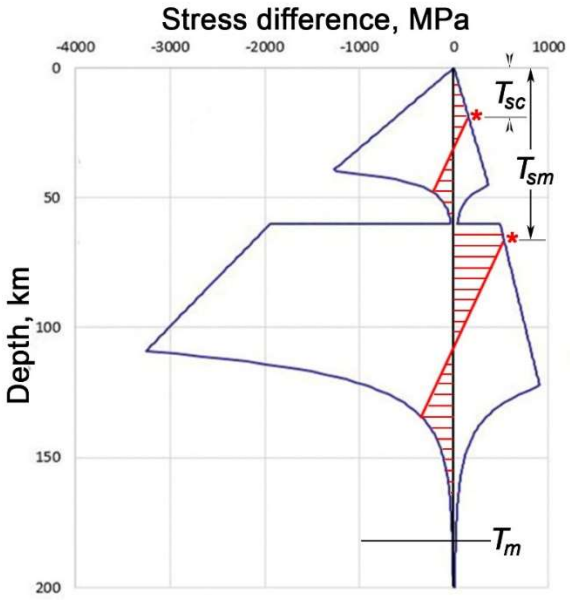

Figure 3. LSE with flexural stresses showing seismicity layer thicknesses in crust T_{sc} and mantle T_{sm}. The overall seismicity laver thickness, i.e. the maximum depth of seismicity, would be Tsm

In summary, the seismogenic layer thickness, Ts, is a parameter that can be measured and should be determined around the InSight landing site if more earthquakes are recorded of sufficient quality to locate their hypocenters. Two models have been used to calculate Ts: the first uses the deepest intersection of differential stress with a brittle section of the *LSE*; the second use the deepest brittle-ductile transition determined in the *LSE*.

5. Example of use of *LSE*s to couple T_e data with T_s

A new map of spatial variations in Te near the InSight landing site and the surrounding regional terrain is shown in Figure 4. Also shown on Figure 4 are centers of three epicenters areas of three events located from the InSight seismic experiment (SEIS, Giardini et al, 2020). The approximate T_es for the two western epicentral areas are 40-45 km: the T_e for the eastern epicentral area is 15-20 km. These events are all in an area where the crustal thickness has been derived to be about 30 km (Figure 4). Giardini et al. (2020) correlate the three seismic events with surface faulting and evidence for young volcanism (tectonic stress localization and/or thermo-elastic cooling),

The seismic data from SEIS (Lognonné et al 2018) provide additional constraints on the lithospheric strength envelopes: From first results (Giardini *et al*., 2020, Clinton *et al.,* 2020), the lack of strong surface waves suggests that the low frequency marsquakes recorded by InSight are more than 30 kilometer deep. Longer observation time and more detailed estimation of source parameters (Brinkman et al., 2020, same issue) will help constrain depths better and separately for more regions. On the other hand, the high frequency events are interpreted as shallow events as the excite guided phases in the crustal layers. Furthermore, receiver functions (Lognonné *et al*., 2020) and noise auto-correlation constrain the crustal velocities and layering. If the crust is

30 km thick, the interpretation of two different depths for the hypocenters recorded in the SEIS experiment indicate that the deeper hypocenters indicate a two-layer *LSE* and are consistent with the Te estimate of 40-45 km from Figure 4.

The T_e from Figure 4 are also consistent with the hypothesis of thermo-elastic cooling (Figure A2A), but if volcanic underplating raised the geotherm too high Te would decrease and Ts would be restricted to the upper crust. We hope that additional data from SEIS will constrain hypocenters and magnitudes so that calculated *LSE*s may be constrained from T_e and T_s.

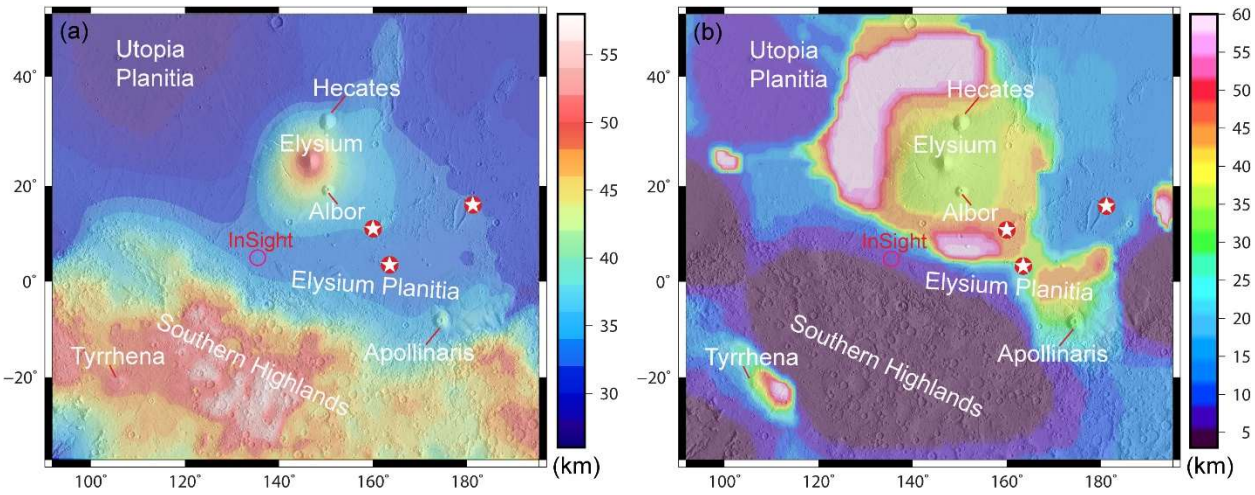

Figure 4 a) Derived crustal thickness, and b) spatial variation of elastic thickness (Te) near the InSight landing site and the surrounding terrain including Elysium Mons (Ratheesh Kumar and Ravat, in preparation; see Appendix for method and parameters). Marsquake putative locations (stars) from Giardini et al. (2020).

6. Concluding Remarks

Lithosphere is an important component of the internal structure of Mars. The term was originally defined for earth by Barrell (1914-15) as a layer with long-term mechanical strength over a weaker layer, the asthenosphere. It has become synonymous with the plates in terrestrial plate tectonics. Mars does not have plate tectonics but Barrell's original definition of the lithosphere is appropriate for Mars. In the absence of pieces of lithosphere moving laterally with respect to each other on Mars (plate tectonics), the question remains how to define the base of the Mars' lithosphere. Assuming that the Mars has continuing motion associated with thermal convection, the Mars' lithosphere would be a single unit with respect to lateral convective motions in the underlying mantle. Underlying the Mars' lithosphere would be a thermal boundary layer which would have a transition in rheology and other physical properties to the convecting mantle. These conditions, which are similar to the base of the terrestrial lithosphere, prevent precise measurement of the base of the lithosphere However, we may learn about the lithosphere and its lateral variations by determining measurable lithospheric physical parameters, such as T_e and T_s.

We have demonstrated above that different techniques used to determine T_e and T_s often

408 measure different physical quantities. In some studies, the different physical quantities result in
409 additional information, but only if one recognizes the implications of each determination.
410 Results from SEIS, the seismic experiment of the InSight lander could place important
411 constraints on T_e and T_s in the vicinity of the lander, and there is still optimism for HP^3, the heat
412 flow experiment. InSight has served to focus much attention on the interior of Mars. We hope
413 that integration of published and new studies of T_e and T_s with a careful understanding of
414 physical implications of the data will bring a new understanding to the Mars' lithosphere.
415
416 **7. Acknowledgments**
417 This work was funded in part by the Colorado Geological Survey and supported by
418 subcontract number 400584 of the InSight Mission from the Jet Propulsion Laboratory. No new
419 data were used in this study. Sources for data in Tables 1 and 2 are given in the table headings.
420 Data source and methodology for preparing Figure 4 are given in the last section of the
421 Appendix. This is InSight contribution number 176.
422

References Cited

Albert, R.A. and Phillips, R.J. (2000) Paleoflexure, *Geophysical Research Letters, **27***, 2385-2388.

Albert, R.A., Phillips, R.J., Dombard, A.J. and Brown, C.D. (2000) A test of the validity of yield strength envelopes with an elastoviscoplastic finite element model, *Geophysical Journal International, **140***, 399-409.

Anderson, D.L., Duennebier, F.K., Latham,G.V., Toksöz, M.F., Kovach, R.L., Knight, T.C.D., Lazarewicz, A.R., Miller, W.F., Nakamura, Y. and Sutton, G. (1976) The Viking seismic experiment, *Science, **194***, 1318-1321.

Azuma, S. and Katayama, I. (2017) Evolution of the rheological structure of Mars, *Earth Planets and Space, **69:8.*** doi10.1186/s40623-016-0593-z.

Barrell, J. (1914/15) The strength of the lithosphere, *J. Geology, **22**,* 28-48; 145-165; 209-236; 289-314; 441-468; 537-555; 655-685; 727-741; ***23***, 27-44; 425-443; 499-515'

Bellas, A., Zhong, S. and Watts, A. (2020) Constraints on the rheology of the lithosphere from flexure of the Pacific plate at the Hawaiian Islands, *Geochemistry, Geophysics, Geosystems, **21***. doi:10.1029/2019Gc008819.

Beardsmore, G.R. and Cull, J.P. (2001) Crustal Heat Flow, A Guide to Measurement and Modelling, *Cambridge University Press*, Cambridge, 324 pp. doi:10.1017/CBO9780511606021.

Blackwell, D.D., Hull, D.A., Bowen, R.G. and Steele, J.L. (1978) Heat flow of Oregon, *State of Oregon, Department of Geology and Mineral Industries, **Special Paper 4***, 45 pp. + map.

Bonner J.L., Blackwell, D.D. and Herrin, E.T. (2003) Thermal constraints on earthquake depths in California, *Bulletin of the Seismological Society of America, **93***, 2333-2354.

Bott, M.H.P and Kusnir, N.J. (1984) The origin of tectonic stress in the lithosphere, *Tectonophysics, **105***, 1-13.

Brace, W.F. (1972) Laboratory studies of stick-slip and their application to earthquakes, *Tectonophysics, **14***, 189-200

Braitenberg, C., Ebbing, J. and Gotze, H.J. (2002) Inverse modelling of elastic thickness by convolution method: the Eastern Alps as a case example, *Earth and Planetary Science Letters, **202***, 387-404.

Braitenberg, C., Wienecke, S. and Wang, Y. (2006) Basement structures from satellite-derived gravity field: South China Sea Ridge, *Journal of Geophysical Research, **111***, doi:10.1029/2005JB003938.

Breuer, D. and Spohn, T. (2003) Early plate tectonics versus single-plate tectonics on Mars: evidence from magnetic field history and crust evolution, *Journal of Geophysical Research, **108***, 8-1 – 8-13. doi:10.1029/2002JE001999.

Broquet, A. and Wieczorek, M.A. (2019) The gravitational signature of martian volcanoes, Journal of Geophysical Research Planets, 124, 2054-2086. Doi/10.1029/2019JE005959.

Broquet, A., Wieczorek, M.A., and Fa, W. (2020) Flexure of the lithosphere beneath the north polar cap of Mars, with implication for ice compositions and heat flow, *Geophysical Research Letters, **47***. doi:10.1029/2019GL086746.

Bryan, S.E. and Ernst, R.E. (2008) Revised definition of large igneous provinces (LIPs), *Earth-Science Reviews, **86***, 175-202.

Burov, E.B. (2010) The equivalent elastic thickness (T_e), seismicity and the long-term rheology of continental lithosphere: time to burn-out "crème brûlée"? Insights from large-scale

geodynamic modeling, *Tectonophysics, **484**,* 4-26.
Burov, E.B. (2011) Rheology and strength of the lithosphere, *Marine and Petroleum Geology, **28***, 1402-1443.
Burov, E.B. and Diament, M. (1995) The effective elastic thickness (T_e) of the lithosphere: what does it really mean? *Journal of Geophysical Research, **100***, 3905-3927.
Byerlee, J.D. (1978) Friction of Rocks, *Pure and Applied Geophysics, **116***, 615-626.
Comer, R.P., Solomon, S.C. and Head, J.W. (1985) Mars: Thickness of the lithosphere from the tectonic response to volcanic loads, *Reviews of Geophysics, **23***, 61-92.
Giardini, D., Lognonné, P., Banerdt, W.B., Pike, W.T. and 59 others (2020) The seismicity of Mars, *Nature Geosciences*. doi:10.1038/s41561-020-0539-8.
Goetze, C. and Evans, B. (1979) Stress and temperature in the bending lithosphere as constrained by experimental rock mechanics. *Geophysical Journal of the Royal Astronomical Society, **59***, 463-478.
Golombek, M.P., Banerdt, W.B., Tanaka, K.L. and Trelli, D.M. (1992) A prediction of Mars seismicity from surface faulting, *Science, **258***, 979-981.
Grott, M. and Breuer, D. (2008) The evolution of the martian elastic lithosphere and implications for crustal and mantle rheology, *Icarus, **193***, 503-515.
Grott, M. and Breuer, D. (2010) On the spatial variability of the martian elastic lithosphere thickness: evidence for mantle plumes? *Journal of geophysical Research, **115***. doi:10.1029/2009JE003456.
Grott, M., Baratoux, D., Hauber, E., Sautter, V., Mustard, J., Gasnault, O., Ruff, S.W., Karato, S.-I., Debaille, V., Knapmeyer, M., Sohl, F., Van Hoolst, T., Breuer, D., Morschhauser, A. and Toplis, M.J (2013) Long-term evolution of the martian crust-mantle system, *Space Science Reviews, **174***, 49-111. doi:10.1007/s11214-012-9948-3
Guest, A. and Smrekar, S.E, (2007) New constraints on the thermal and volatile evolution of Mars, *Physics of the Earth and Planetary Interiors, **164***,161-176.
Hauck, S.A., II, and Phillips, R.J. (2002) Thermal and crustal evolution of Mars, *Journal of Geophysical Research, **107***. doi: 10.1029/2001JE001801.
Jamison, D.B. and Cook, N.G.W. (1980) Note on measured values for the state of stress in the earth's crust, *Journal of Geophysical Research, **85***, 1833-1838.
Jimenez-Diaz, A., Egea-Gonzalez, I, Parro, L.M., Tasaka, M. and Ruiz, J. (2020) The thermal structure and mechanical behavior of the Martian lithosphere, Icarus. doi:10.1016/j.icarus.2020.113635
Kiefer, W.S. and Li, Q. (2009) Mantle convection controls the observed lateral variations in lithospheric thickness on present-day Mars, Geophysical Research Letters, **36**, doi:10.1029/2009GL039827.
Knapmeyer, M., Oberst, J., Hauber, E., Wählisch, M., Deuchler, C. and Wagner, R. (2006) Working models for spatial distribution and level of Mars' seismicity, *Journal of Geophysics Research, **111***. doi:10.1029/2006JE002708.
Kohlstedt, D.L., Evans, B., Mackwell, S.J. (1995) Strength of the lithosphere: constraints imposed by laboratory experiments, *Journal of Geophysical Research, **100***, 17587-17602.
Kronberg, P., Hauber, E., Grott., M., Werner, S.C., Schäfer, T., Gwinner, K., Giese, B., Masson, P and Neukum, G. (2007) Acheron Fossae, Mars: tectonic rifting, volcanism and implications for lithospheric thickness, *Journal of Geophysical Research, **112***. doi:10.1029/2006JE002780.
Kusnir, N.J. and Park, N.J. (1984) Intraplate deformation and the strength of the lithosphere,

Geophysical Journal of the Royal Astronomical Society, 79, 513-538.
Lognonné, P., Banerdt, W.B., Pike, W.T., Giardini, D., and 59 others (2020) Constraints on the shallow elastic and anelastic structure of Mars from InSight seismic data, Nature Geosciences. doi:10.1038/s41561-020-0536-y.
McCubbin, F.M., Smirnov, A., Nekvasil, H., Wang, J., Hauri. and Lindsley, D.L. (2010) Hydrous magmatism on Mars: a source of water for the surface and subsurface during the Amazonian, Earth and Planetary Science Letters, 292, 132-138.
McGarr, A. (1980) Some constraints on levels of shear stress in the crust from observations and theory, *Journal of Geophysical Research, **85***, 6231-6238.
McGovern, P.J., Solomom, S.C., Smith, D.E., Zuber, M.T., Simons, M., Wieczorek, M.A., Phillips, R.A., Neumann, G.A., Aharonson, O. and Head, J.W. (2002) Localized gravity/topography admittance and correlation spectra on Mars: Implications for regional and global evolution, *Journal of Geophysical Research, **107***. doi:10.1029/2002JE001854.
McGovern, P.J., Solomom, S.C., Smith, D.E., Zuber, M.T., Simons, M., Wieczorek, M.A., Phillips, R.A., Neumann, G.A., Aharonson, O. and Head, J.W. (2004) Correction to localized gravity/topography admittance and correlation spectra on Mars: Implications for regional and global evolution, *Journal of Geophysical Research, **109***. doi:10.1029/2004JE002286.
McNutt, M.K. (1984) Lithospheric flexure and thermal anomalies, *Journal of Geophysical Research, **89***, 11,189-11,194.
Morgan, P., Blackwell, D.D., Spafford, R.E. and Smith, R.B. (1977) Heat flow measurements in Yellowstone Lake and the thermal structure of the Yellowstone Caldera, *Journal of Geophysical Research, **82***, .3719-3732.
Morschhauser, A., Grott, M. and Breuer, D. (2011) Crustal recycling, mantle dehydration, and the thermal evolution of Mars, *Icarus, **212***, 541-558.
Mysen, B.O., Virgo, D., Popp and Bertka, C.M. (1998) The role of H_2O in martian magmatic systems, *American Mineralogist, **83***, 942-946.
Phillips, R.J. (1991) Expected rates of marsquakes, in Scientific Rationale and Requirements for a Global Seismic Network on Mars, *Lunar and Planetary Institute Technical. Report. **91-02***, 13-15, Houston, Texas.
Plesa, A., Tosi, N., Grott, M and Breuer, D. (2015) Thermal evolution and Urey ration of Mars, *Journal of Geophysical Research, **120***. doi:10.1002/2014JE004748.
Plesa, A., Grott, M., Tosi, N., Breuer, D., Spohn, T. and Wieczorek, M.A. (2016) Haw large are present-day heat flux variations across the surface of Mars? *Journal of Geophysical Research, **121***. doi:10.1002/2016JE005126.
Plesa, A., Knapmeyer, M., Golombek, M.P., Breuer, D., Grott, M., Kawamura, T., Lognonné, P., Tosi, N. and Weber, R.C. (2018) Present-day Mars' seismicity predicted from 3-D thermal evolution models of interior dynamics, Geophysical Research Letters, 45, 2,580-2,589. doi:10.1002/2017GL076124.
Ranalli, G. and Murphy, D.C. (1987) Rheological stratification of the lithosphere, *Tectonophysics, **132***, 281-295.
Ruiz, J., Gomez-Ortiz, D. and Tejero, R. (2006a) Effective elastic thickness of the lithosphere in the Central Iberian Peninsula from heat flow: implications for the rheology of the continental lithosphere, *Journal of Geodynamics, **41***, 500-509.
Ruiz, J., Fernandez, C., Gomez-Ortiz, D., Dohm, J.M., López, V. and Tejero, R. (2006b) Ancient heat flow, crustal thickness, and lithospheric mantle rheology in the Amenthes

region, Mars, *Earth and Planetary Science Letters,* ***270***, 1-12.
Solomon, S.C. and Head, J.W. (1990) Heterogeneities in the thickness of the elastic lithosphere of Mars: constraints on heat flow and internal dynamics, *Journal of Geophysical Research,* ***121***, 11,073-11,083.
Stetsky, R.M. (1978) Rock friction - effect of confining pressure, temperature, and pore pressure, *Pure and Applied Geophysics,* ***116***, 690-704.
Tapponier, P. and Francheteau, J. (1978) Necking of the lithosphere and the mechanics of slowly accreting plate boundaries, *Journal of Geophysical Research,* ***83***, 3955-3970
Taylor, R.S. and McLennan, S.M. (2009) Planetary Crusts: Their Composition, Origin and Evolution, *Cambridge University Press*, Cambridge, 378 pp.
Taylor, J., Teanby, N.A. and Wookey, J. (2013) Estimates of seismic activity in the Cerberus Fossae region of Mars, *Journal of Geophysical Research: Planets,* ***118***, 2570-2581. doi:10.1002/2013JE004469.
Turcotte, D.L. and Schubert, L. (1982) Geodynamics, applications of continuum physics to geological problems, *Wiley*, New York, 450 pp.
Watts, A.B. (2001) Isostasy and flexure of the lithosphere, *Cambridge University Press*, Cambridge, 458 pp.
Watts, A.B. and Burov, E.B. (2003) Lithospheric strength and its relationship to the elastic and seismogenic layer thickness, *Earth and Planetary Science Letters,* ***213***, 113-131.
Weertman J. and Weertman, J.R. (1975*)* High temperature creep of rock and mantle viscosity, *Annual Reviews of Earth and Planetary Sciences,* ***3***, 293-315.

583 **Table 1**. Summary of T_e estimates from admittance method (modified from McGovern et al.,
584 2004)

Feature	Surface Age[a]	T_e, km	Thermal gradient, K/km	Heat flow, mW/m^2
Olympus Mons[b]	A	>70	<8	<24
Ascraeus Mons[b,d]	A	2-80	5-55	13-140
Pavonis Mons[b,d]	A	<100	>5	>13
Arsia Mons[b,c]	A	>20	<10	<28
Alba Patera[b,c]	A - H	38-65	5.5-16	16-40
Elysium Rise[b]	A - H	15-45	6-13	15-33
Hebes Chasma[e]	A - H	>60	<10	<28
Hebes Chasma[e,f,g]	A - H	60-120	5-9	17-25
Candor Chasma[e]	A - H	>120	<6	<20
Candor Chasma[e,f,g]	A - H	80-120	3-7.5	11-23
Capri Chasma[e]	A - H	>110	<6	<20
Capri Chasma[e,f,g]	A - H	>100	<7	<23
Solis Planum[e,h]	H	24-37	8-14	20-35
Hellas south rim[e,h]	H - N	20-31	10-16	25-40
Hellas south rim[d,e,i]	H - N	40-120	6-11	20-28
Hellas west rim[e,h]	H - N	<20	>12	>30
Hellas basin[e,h]	N	<13	>14	>35
Noachis terra[e,h]	N	<12	>20	>50
Northeastern Terra Cimmeria[e,h]	N	<12	>19	>48
Northeastern Arabia Terra[e,h]	N	<16	>17	>43

585 [a] letters A, H and N refer to Amazonian, Hesperian and Noachian epochs, respectively.
586 [b] Crustal density taken to be equal to nominal value (2,900 kg/m^3).
587 [c] Best fit density
588 [d] Parameter ranges reflect the possibility that lithospheric ductile strength may be limited by
589 that of either olivine or diabase.
590 [e] Crustal density taken to equal that of load density.
591 [f] Load density varied in increments of 100 kg/m^3.
592 [g] Alternate solution with low surface density.
593 [h] Ductile strength taken to be that of diabase.
594 [i] Alternate solution with bottom loading.
595
596

597 **Table 2**. Volcanic load information and estimates of elastic lithosphere thickness, T_e. Data from
598 Comer et al. (1985)

Load feature	Excess mass, x10^{21} kg	Rille distances		Lower bound, km	Best fit, km	Upper bound, km
		r_{in}, km	r_{out}, km			
Ascraeus Mons	2.1	170 ± 30	250 ± 20	8	22	50
Pavonis Mons	1.3	150 ± 30	230 ± 30	10	26	50
Arsia Mons	2.3	170 ± 40	260 ± 50	10	18	50
Alba Patera	2.8	200 ± 25	350 ± 50	19	33	85
Elysium Mons	0.5	150 ± 20	350 ± 20	48	54	110
Olympus Mons	8.7	…	…	150	200(?)	…
Isidis Palitia	…	…	…	120	200-300(?)	…

599

600

Appendix

Calculation of Model *LSE*s

LSE calculations are based on the results of laboratory experiments and models of rock deformation. A recent detailed description that is relevant to the methods used here was given by Jiminez-Diaz *et al*. (2020). The yield strength of the lithosphere at any depth is given by the lesser of the brittle and ductile yield strengths [Tapponier and Francheteau, 1978; Goetze and Evans, 1979; Weertman and Weertman, 1979]. Evidence suggests that crustal rocks are extensively fractured [Brace, 1972] and thus, for brittle failure, rock is modeled as a frictional plastic material. Resistance to sliding on fractures increases with pressure, and thus depth and regional stress, but appears to be generally independent of strain rate, temperature, and rock composition [Byerlee, 1978; Jamison and Cook, 1980; McGarr, 1980; Stetsky, 1978]. The brittle yield strength at depth z is calculated by (modified from Ruiz *et al*., 2006a, b):

$$(\sigma_1 - \sigma_2)_z = \int_0^z \alpha\rho(z)g \text{ z.dz} \quad \text{(A1)}$$

where $(\sigma_1 - \sigma_2)_z$ is the difference between the maximum and minimum stresses at depth z, α is a factor depending on the stress regime (0.75 for extension and 3 for compression: Ranalli and Murphy, 1987), ρ(z) is density at depth z, and g is acceleration due to gravity.

For ductile strength we have assumed a power-law, steady-state creep equation of the form:

$$(\sigma_1 - \sigma_2)_z = (\dot{\varepsilon}/\dot{\varepsilon}_0)^{1/n} exp[Q^*/3R\Theta] \quad \text{(A2)}$$

where ε̇ is strain rate, P is pressure, Q^* is activation energy, R is the gas constant, Θ is absolute temperature, and $\dot{\varepsilon}_0$ and n are constants dependent on rock composition. The brittle and ductile strength equations used here predict a brittle-ductile transition at a temperature of 400-450°C (~675-725 K) for mafic lower continental crust. There are many assumptions inherent in these equations and improvements have been published ([*e.g*., Kohlstedt *et al*., 1995). However, as shown in Figure A1, the predicted brittle-ductile transition temperature reasonably predicts the cutoff depth of terrestrial continental seismicity hypocenter depths: thus, the equations are assumed to be useful for modeling *LSE*s for Mars. There is uncertainty in the water content of the Mars upper mantle and some authors use upper mantle creep parameters for both wet and dry rheologies. This subject is discussed by Grott et al. (2013). Some studies conclude that the water content could be as low as 1-36 ppm water (Mysen et al., 1998). In contrast other studies argue for water contents of 55 to 220 ppm (McCubbin et al., 2010), values similar to the water content in earth's mantle. Creep parameters that have been successfully used to model terrestrial lithospheric rheology are representative of a dry rheology (*e.g*., Bellas et al. 2020) and we have used similar dry rheology mantle parameters here.

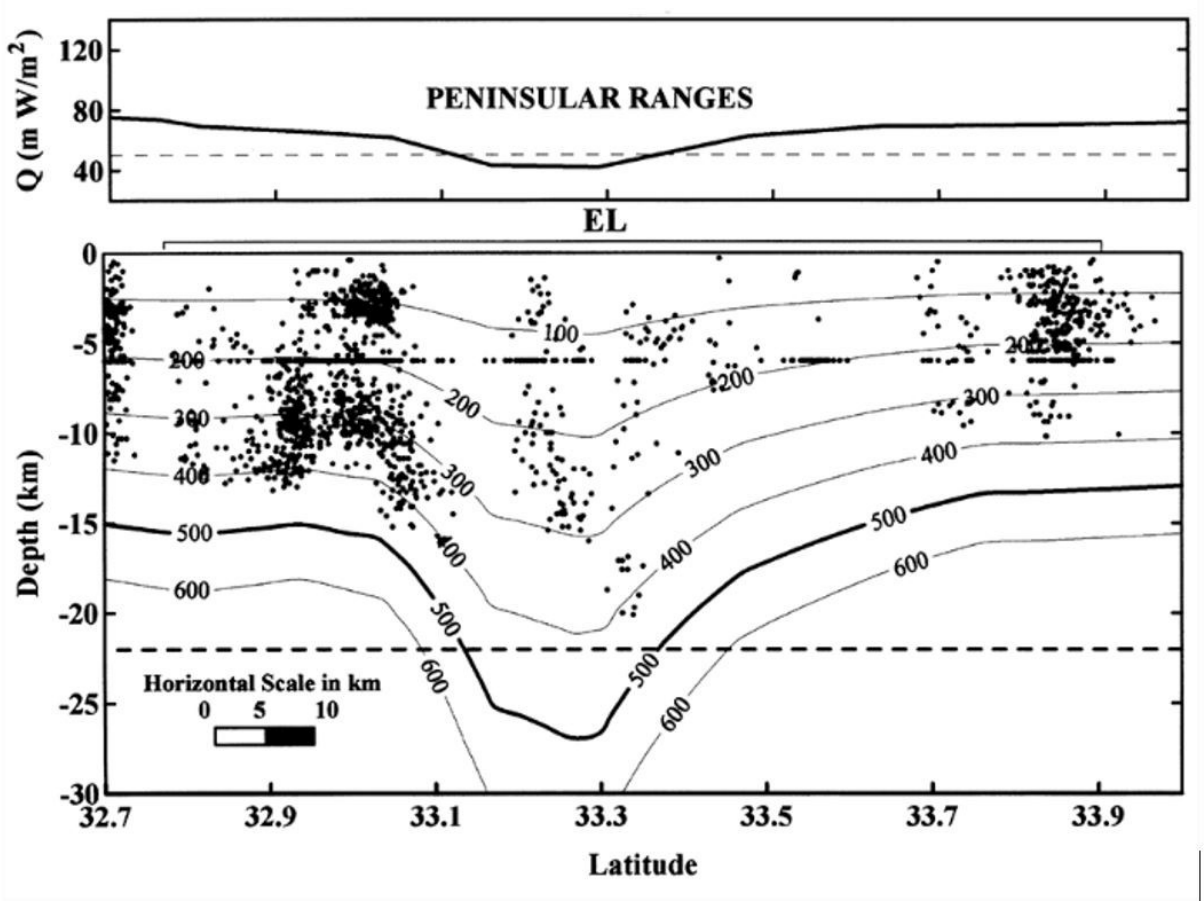

Figure A1. Cross-section showing temperatures and earthquake depths across the Peninsula Ranges, California, USA. Profile trends roughly west to east at latitude 32.3°N along the Elsinore Fault zone (EL). Q is heat flow (modified from Bonner *et al*., Figure 7).

Mars Model *LSE*s

Model *LSE*s were calculated for Mars using the equations above, assuming a surface temperature of 218 K (approximate InSight landing site mean annual ground temperature) and the following parameters for ductile deformation:

Table A1. Parameters used for ductile deformation in calculation of LSEs for this study.

Composition	log $\dot{\varepsilon}_0$	n	Q*
Mafic	-1.2 ± 1.2	3.05	276000 ± 21
Ultramafic	4.5 ± 0.1	3.60	535000 ± 21

The crust was assumed to have a mafic composition and the mantle to have a heat production of 0.01 μW/m^3 down to a depth of 250 km. A basaltic composition was assumed for the crust with a thermal conductivity of 2 W/(m K) (Beardsmore and Cull, 2001), and the mantle was assumed to have a temperature-dependent olivine conductivity. Twenty per cent of surface heat flow was assumed to originate from conduction through the base of the crust with 80% generated in the

crust by radiogenic heat production. Crustal thickness and surface heat flow were variables. Theoretical Mars geotherms were calculated using the parameters given above for crustal thicknesses of 30 and 60 km. For each crustal thickness surface heat flow was varied from 5 to 80 mW/m^2 in increments of 5 mW/m^2.

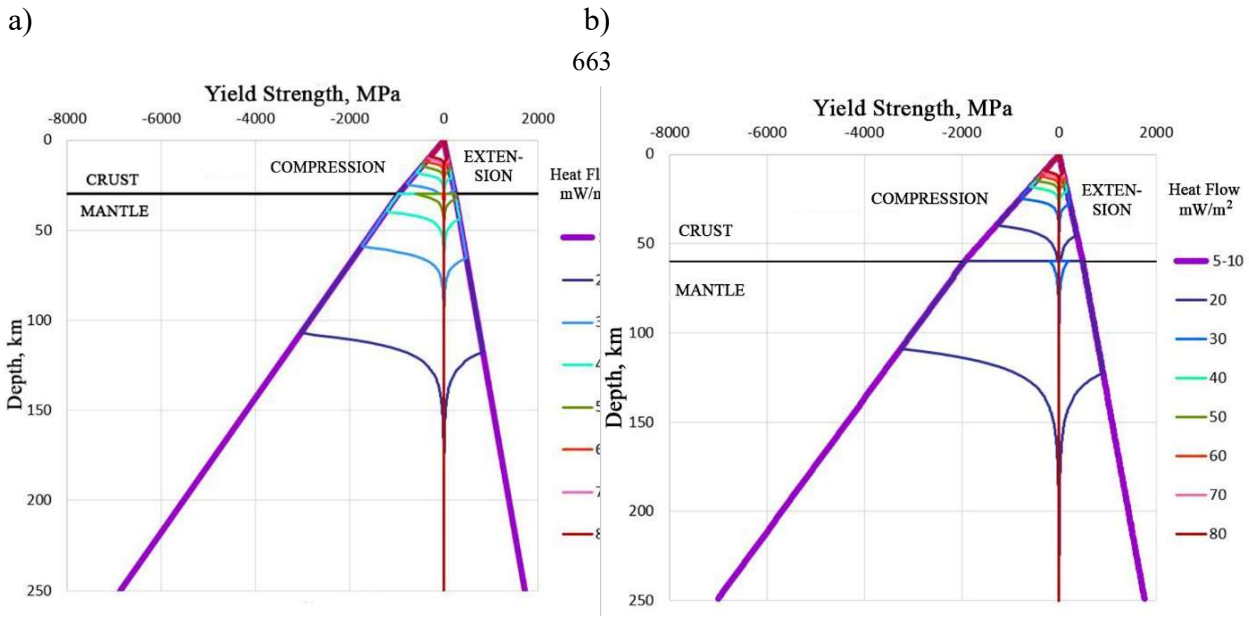

Figure A2. *LSE*s calculated for a). 30 km-thick and b) 60 km-thick crusts. See text for parameters and equations used to calculate curves.

*LSE*s were calculated for a selection of the calculated geotherms for both crustal thicknesses are shown in Figure A2. Linear sections of the curves indicate brittle strength; non-linear sections indicate ductile strength. For low surface heat flow the strength to a depth of 250 km is all brittle; the junctions between the non-linear and linear sections of the curves are the brittle-ductile transitions. There is often a discontinuity in the curves at the crust-mantle boundary corresponding to compositional change. Ductile strength curves were calculated using a strain rate of 10^{-22} s^{-1} (see below). As surface heat flow increases for a 30 km-thick crust, a ductile zone appears first in the mantle, and then at 30 mW/m^2 in the lower crust. For a 60 km-thick crust, a ductile zone appears first in the lower crust at a surface heat flow of about 20 mW/m^2. These *LSEs* are not intended to represent specific times or locations on Mars, but are families of curves that are illustrative of the effects of changes in crustal thickness and surface heat flow.

A wide range of strain rates have been used to calculate ductile strength for *LSE*s ranging from 10^{-14} s^{-1} (Plesa et al., 2016) to 10^{-19} s^{-1} (McGovern et al., 2002, 2004). We have chosen a very conservatively slow strain rate of 10^{-22} s^{-1} for ductile strength calculations here in order to maximize the number of brittle-ductile transitions in the LSEs in the surface heat-flow range tested. With the low Mars' surface temperature for the geotherms (218 K used in these calculations) the LSEs showed only brittle failure above 250 km in the lower range of the heat-flow increments tested with the higher strain rates. In terms of ductile strengths, although there

686 is eight order of magnitude in strain rate under consideration here (10^{-14} to 10^{-22} s^{-1})) the resulting
687 change in ductile strength is only a factor of 167 (factor obtained by calculating $(\dot{\varepsilon}/\dot{\varepsilon}_0)^{1/n}$ from
688 equation A2 for strain rates of 10^{-14} s^{-1} and 10^{-22} s^{-1} and taking the ratio). Thus, large changes in
689 strain rate have major geological implications and important consequences for depths to brittle-
690 ductile transitions, but are very subdued in terms of ductile strength.
691
692 **Relationship Among *LSE*s, Seismogenic and Elastic Layer Thicknesses**
693 Rheology is a term that implies time and the three definitions of lithospheric rheology
694 discussed here all operate at different time-scales. *LSE*s are calculated on the assumption that
695 stress is applied to the lithosphere instantaneously with a constant strain rate in the plane of the
696 stress direction where ductile strain dominates. The strain rate used for terrestrial calculations is
697 typically of the order of 10^{-15} s^{-1} for terrestrial strength calculations and we have used 10^{-22} s^{-1} for
698 Mars calculations. The seismogenic layer is the relatively shallow depth zone in which
699 seismicity (earthquakes or marsquakes) is restricted. It is an indication of brittle failure in the
700 lithosphere. Deformation resulting in earthquake signals occurs on timescales or the order of
701 seconds to minutes. There is no evidence that slow earthquakes occur on Mars but, should they
702 occur, the timescale could be hours to months. Lithospheric flexure is a response of the
703 lithosphere to long-term ($\geq 10^5$ yr) geologic loads (Watts and Burov, 2003). Gravity and
704 topography data from, which T_e has been determined by the admittance method, were generally
705 collected on timescales of the order of gigayears after loading, the exception being ice loading at
706 the poles (*e.g.* Broquet et al., 2020)
707 T_e and T_s for flexure in a uniform composition lithosphere is shown in Figure A3A. As
708 discussed above, there are more than one interpretation of T_e possible. A deviatoric stress line
709 crosses each segment of the *LSE* so that is defines equal areas in the compression and extension
710 portions of the *LSE* segment. Where this line crosses the ordinate axis is the neutral stress depth.
711 From Newton's Second Law, the elastic strength is the effective sum of the areas in the *LSE*
712 between the deviatoric stress line, the ordinate axis, and the *LSE*, Other portions of the *LSE* are
713 not included in the elastic core because they are not stressed. T_s is simpler as there is only one
714 maximum depth of the brittle yield strength, assuming that the LSE and flexural stress are
715 calculated correctly. With a multilayer lithosphere interaction of flexural stresses with the LSEs
716 for each layer become more complex, as shown in Figure A3B. If the lower limit of ductile
717 strength separates the layers they become mechanically separated and each layer has an
718 individual elastic core (Burov 2010, 2011). The effective elastic thickness then is the combined
719 effect of the individual elastic cores.
720

721 a) b)

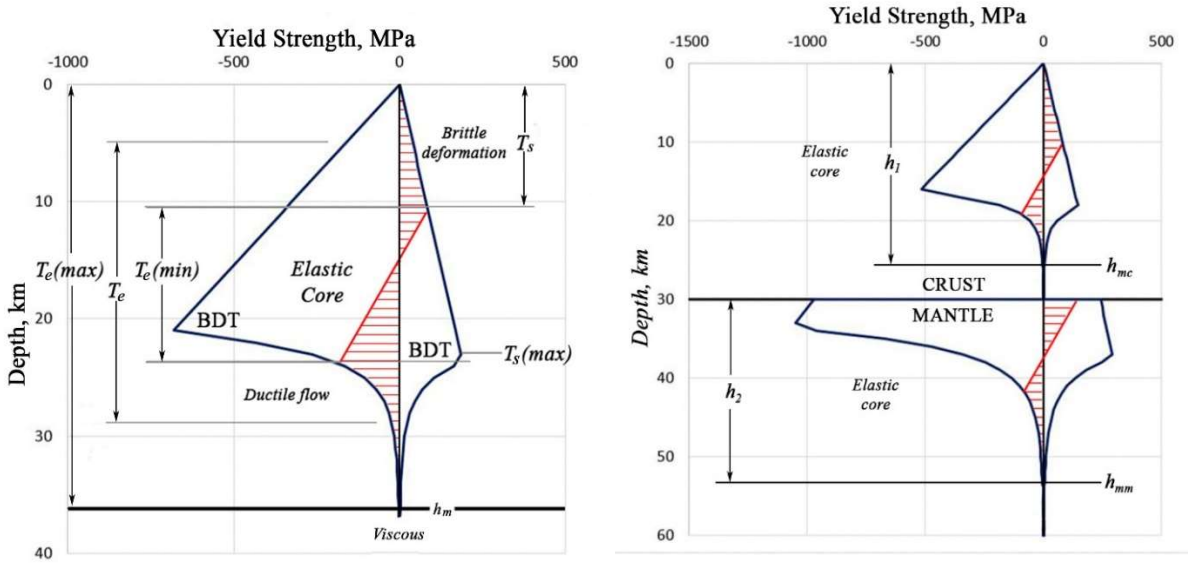

723

724 **Figure A3**. A) Mars *LSE* for a uniform lithosphere showing possible relationships of effective
725 elastic lithosphere depth ranges (T_e) and depths of layer of seismicity (T_s). The red dashed
726 lines indicate stresses associated with flexure [Adapted from Burov (2010)]. b) *LSE* for a
727 layered Mars lithosphere. Thicknesses of the elastic cores of the two layers, h_1 and h_2 are
728 indicated [Adapted from Burov (2010)].

729

730 Burov and Diament (1995) indicate that the addition of a uniform horizontal stress to the
731 lithosphere shifts the deviatoric stress areas in the curves in Figure A7 either to the left
732 (compression) or to the right (extension) according to the sign of the external stress. Watts and
733 Burov (2003) state that if the layers in the *LSE* are decoupled, the elastic strength reflects the
734 strength in each elastic layer; It is not simply the sum of the thicknesses of the layers (h_1, h_2, …
735 h_n) but is given by the Kirchov relation:

736

737 $$T_e \approx \left({h_1}^3 + {h_2}^3 + \ldots + {h_n}^3\right)^{1/3} = \left(\sum_{i=1}^{n} {h_i}^3\right)^{1/3} \quad \text{(A3)}$$

738

739 An example of a Mars *LSE* is shown in Figure A4 with elastic and seismogenic layer
740 thicknesses with a uniform horizontal regional stress field. This is based on our interpretation of
741 the application of a uniform horizontal regional stress to the flexure model by Burov and
742 Diament (1995). As discussed in the caption for this figure, a two-layer *LSE* is predicted under
743 these conditions, as with the flexure model, but the seismogenic layer thickness is limited to the
744 upper crust unless the magnitude of the regional stress field exceeds the mantle brittle strength at
745 the crust-mantle boundary (Moho). These results are robust for this type of *LSE* model yielding
746 the conclusion that for Mars, elasticity in the lithosphere is generally distributed over at least two
747 layers, one in the crust and one in the mantle, depending on crustal thickness and heat flow,
748 seismicity may be limited to the crust or be in two zones, one in the crust and one in the upper
749 mantle.

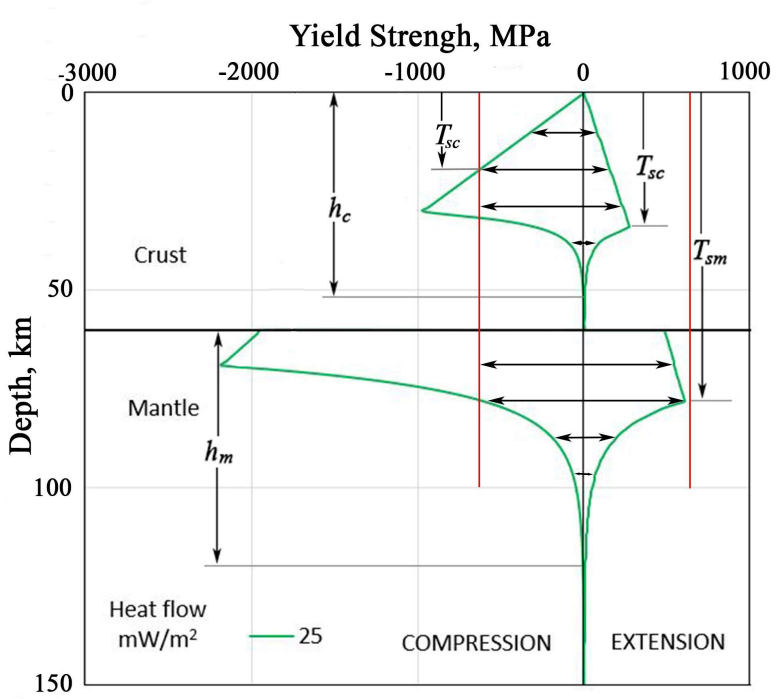

Figure A4. *LSE* for Mars calculated for a 60 km thick. Assuming uniform horizontal regional stresses maximum thicknesses of elastic zones have been shown for the crust (h_c) and the mantle (h_m). In extension the external stress is shown to exceed the maximum brittle ductile yield strengths, the crustal and mantle seismogenic layer thicknesses, T_{sc} and T_{sm}, respectively, are defined by the depths to the brittle ductile transitions. Unlike flexure of the lithosphere where the applied deviatoric stress is represented by a sloping line through the plot, a uniform external stress is represented by a vertical line at the magnitude of the applied stress. The elastic strength is the area between the brittle ductile curve for extension and the ordinate axis. He external uniform stress does not exceed the brittle-ductile transition in either the crust or the mantle in compression and does not cross the brittle curve in the mantle. Thus, the seismogenic layer thickness under compression is the depth at which the external stress line crosses the crustal brittle curve under compression. The elastic strength is the area between the brittle ductile curve for compression, the external stress line and the ordinate axis.

Method of calculation of T_e for Figure 4

Figure 4 shows the spatial variation of crustal and elastic thickness near the InSight landing site and surrounding regions prepared by Ratheesh-Kumar & Ravat using the space domain convolution method developed by Braitenberg et al. (2002, 2006). The method assumes that the bending of the Moho is caused by topographic loads using thin plate and point load approximations (Turcotte & Schubert, 1982; Watts, 2001). The topography and Bouguer gravity models were from the MOLA team and Genova et al. (2016), respectively, from PDS. The Bouguer model is spherical harmonic degree 90 (minimum wavelength ~ 240 km) and because the region contains large volcanic provinces, windows of 1000 x 1000 km, offset by 60 km throughout the region were used to estimate elastic thickness shown in Figure 4b. The

776 convolution method is not affected by spectral tapering uncertainties and consideration of limited
777 spectral range for the fit between observed and computed spectra; however, the resolution of its
778 elastic bending response kernels for large elastic thicknesses is limited and the results depend on
779 how well the flexure-based Moho approximates the Bouguer anomaly Moho using downward
780 continuation of the signal (similar to Wieczorek & Phillips, 1998). Another limitation of the
781 method is that, presently, it operates in rectangular coordinates; however, since the Bouguer
782 gravity anomalies are based on spherical computations, the only approximation involved is the
783 distortion of the length of spherical arc upon flattening, which is less than 3 km for the 500 km
784 half-window (over which the distortion occurs) and thus the results are not affected in
785 comparison to all of the assumptions involved in the calculations of elastic thickness by any
786 available method. Results from Broquet & Wieczorek (2019) suggest that ignoring intra-crustal
787 and mantle loads in the calculations did not significantly change the estimates of elastic thickness
788 for most regions they studied, including the large Elysium volcanic region